# Trabajo Final de Máster

Máster en Zoonosis y One Health

# Immunohistochemical comparative study between two strains of the Chikungunya virus in a mouse model


Autora

Nuria Pérez Fernández

Directores

Enric Vidal

Núria Busquets

Tutora

Natàlia Majó

**Universidad Autónoma de Barcelona**

**Facultad de Veterinaria**


**Septiembre 2018**

## Acknowledgments

I would like to thank my directors Enric Vidal and Núria Busquets for their help in carrying out this work. On the other hand, I would like to thank the pathological anatomy staff of CReSA, thanks to their help I have been able to learn new laboratory techniques and it has been possible to carry out the present study properly.

## List of abbreviations

| Term | abbreviation |
|---|---|
| Chikungunya virus | CHIKV |
| East Central South Africa | ECSA |
| Indian Ocean islands | IOLs |
| Interferon | IFN |
| Intradermal | ID |
| Intravenous | IV |
| Wild type | WT |
| Central nervous system | CNS |
| Days post inoculation | DPI |
| 3-3’ diaminobenzidine | DAB |
| Bovine serum albumin | BSA |
| Immunohistochemistry | IHQ |

# Contents

## Abstract

Chikungunya fever is a vector-borne disease caused by Chikungunya virus (CHIKV) that is transmitted mainly through the bite of *Aedes aegypti* and *Aedes albopictus* mosquito species. Nowadays there is no prophylaxis for CHIKV and it has been responsible of several major outbreaks since the 2000s such as La Réunion island outbreak in 2005. These diverse outbreaks have allowed the spread of the virus to different parts of the world to such an extent that autochthonous outbreaks have been confirmed in Europe. Climate change, imports from endemic areas and the adaptation of arboviruses to novel vectors could produce more outbreaks in the future and colonization of new places by mosquitoes carrying the virus. In this project, a comparative study between two different CHIKV strains (S27 and ITA1) in an IFN-α/β $^{(-/-)}$ receptor knock out mice model was carried out in order to characterize the tropism of the virus. Immunolabeling was found in joints (synovial capsule), fibrocytes (periosteum, epineurium, endo/perimysium, blood vessel's basal lamina, and dermis), macrophages (in the spleen, lymph nodes and liver's kupffer cells), endothelium, leptomeningeal cells and some foci in the glia of the encephalon, among others. However, nonspecific immunolabeling has also occurred in some control tissues requiring careful evaluation. The immunolabelling differences between the two strains were not very noticeable. Clinically, the S27 strain was more virulent and the ITA1 strain caused a greater lympholysis. The development of studies about the pathogenesis of different CHIKV strains in animal models helps obtaining a better understanding of the pathophysiology of the disease and, therefore, will be useful in the search for new therapies and vaccines to prevent and control the disease.

# 1. Introduction

## 1.1 Chikungunya fever: origin of the zoonosis and public health concern

Chikungunya fever is an acute febrile disease that is caused by an arthropod-borne alphavirus, Chikungunya virus (CHIKV), and it is transmitted to humans through the bite of *Aedes* mosquitoes (Staples *et al*., 2009). CHIKV was first identified in the early 1950s, during an outbreak in the Makonde Plateau region of Tanzania, and since then some cases have been identified in many countries around the world, mainly in Africa and Asia. CHIKV is maintained in Africa by mosquitoes that live in forests and bite wild primates. The name Chikungunya is derived from a Makonde or Swahili word meaning "disease that bends up the joints" and refers to the flexed posture of those infected with the virus (Burt *et al*., 2017). Since the 2000s it has re-emerged to infect millions of people across the world, especially in Africa, Asia and Oceania, becoming a major global public health concern. There is not a specific cure for this disease despite the advances in the knowledge of the pathophysiology and the virus itself so far. In the future there could be more outbreaks in other parts of the world that have never had the disease, due to imports from endemic areas or because mosquitoes carrying the virus invade these new areas as a consequence of climate change.

## 1.2 Epidemiology, expansion and evolution of CHIKV

The transmission of CHIKV occurs through the bite of infected *Aedes aegypti* or *Aedes albopictus* mosquito species, although in recent epidemics some cases were the result of maternal-fetal transmission (Schwartz and Albert, 2010). *Aedes aegypti* is found in tropical and subtropical regions while, *Aedes albopictus* is more widely distributed, since it can even be found in temperate zones (Burt *et al*., 2017). Chikungunya fever is a **zoonosis**, that is, it is transmitted from animals to humans through these vectors. The virus can be transmitted through two different cycles: urban and sylvatic (figure 1). The urban cycle refers to the transmission of human to mosquito to human, however, the sylvatic cycle refers to the transmission between animal and mosquito. The sylvan cycle is the main form of CHIKV maintenance in Africa by mosquitoes that live in forests and wild primates. However, in the most densely populated areas, it is mainly maintained in an urban cycle, in which humans act as the main hosts and mosquitoes of the *Aedes* genus act as vectors (Ganesan *et al*., 2017).

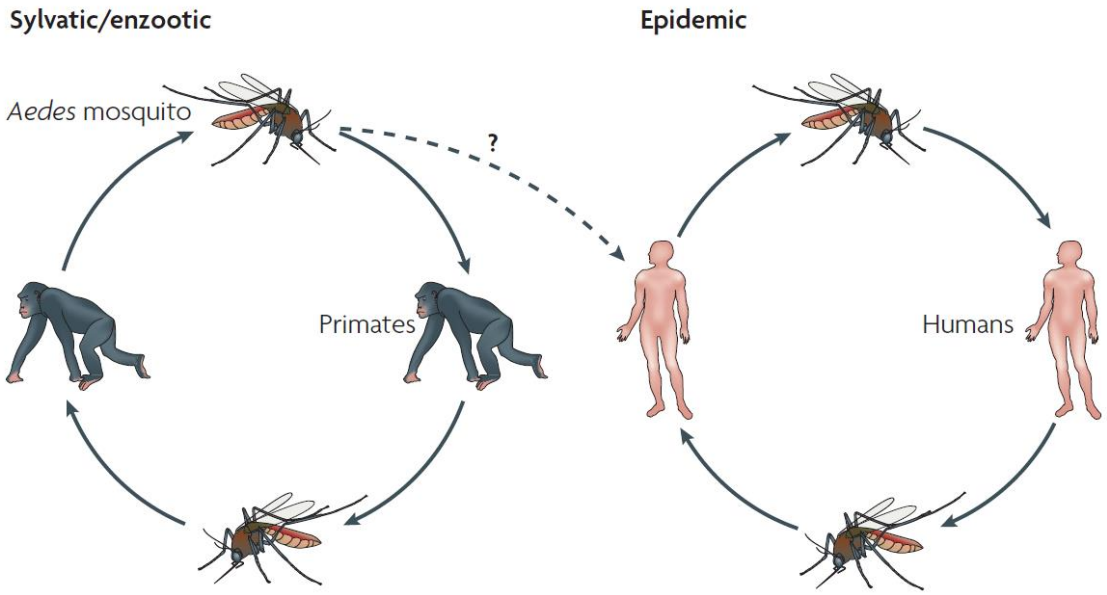


**Figure 1.** CHIKV sylvatic cycle maintained by mosquitoes that live in forests and wild primates and CHIKV urban cycle, where humans are the main host. (Whitehead *et al*., 2007).

CHIKV probably was originated in Central/East Africa, and was first reported in Tanzania in 1952 (Wahida *et al*., 2017) where it has been discovered that the virus circulates in a sylvatic cycle. In these areas, sporadic human cases occur, but large human outbreaks are infrequent. The first significant outbreaks of Chikungunya fever occurred in the 60s in several areas of Asia such as Thailand and India (Staples *et al*., 2009); however, there have been no further outbreaks in the following years until the decade of the 2000s. Since the year, 2000 Chikungunya outbreaks have occurred due to the spread of the virus to regions that were not previously endemic.

In 2004, a large epidemic began on the coast of Kenya with almost half a million cases reported (Wahida *et al*., 2017). This outbreak caused the CHIKV spreading to numerous islands in the Indian (figure 2) (Burt *et al*., 2017). In addition, at least 18 countries in Asia, Europe and North America documented imported cases of Chikungunya fever, and some of these countries developed local autochthonous transmission of the virus (Staples *et al*., 2009). In 2005, movement of goods and people among the islands of the Indian Ocean led the introduction of CHIKV into La Réunion Island causing one of the biggest outbreaks in recent decades with 40,000 cases reported per week. It is believed that this outbreak was transmitted by *Ae. albopictus* and also, was the first time that a number of neurological manifestations, fetal infections and mortality were reported to be associated with CHIKV (Staples *et al*., 2009).

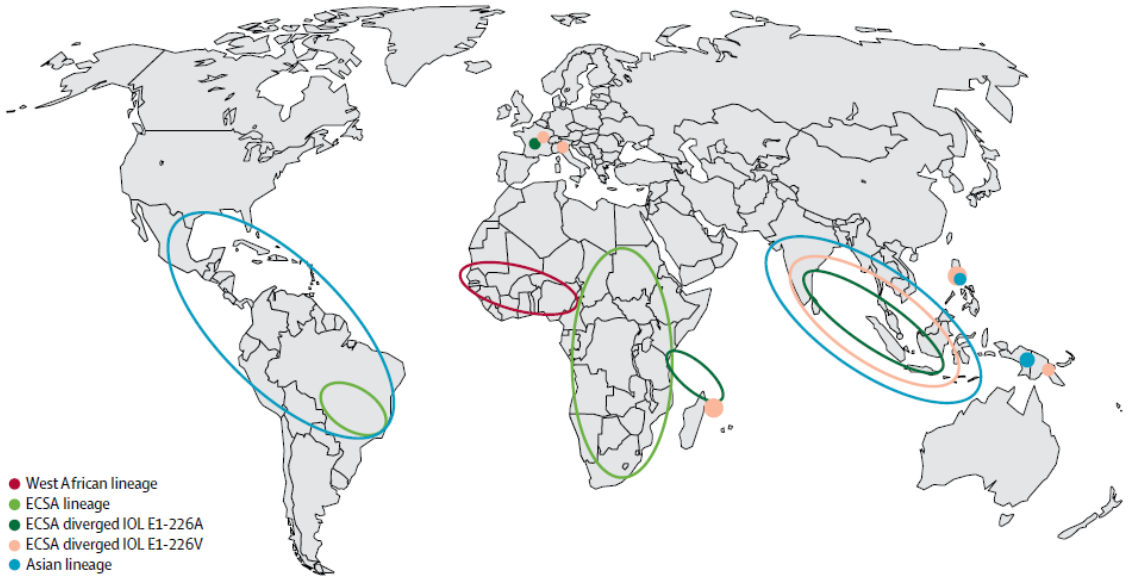


**Figure 2.** Spread and divergence of the East Central South African (ECSA) genotype to the Indian Ocean islands (IOLs) and Asia. The spread of the Asian lineage to the Americas in 2013, and the spread of the ECSA lineage to South America in 2014. Autochthonous cases identified in Europe and their genetic lineage are shown (Burt *et al*., 2017).

During 2006–2010, ECSA (East Central South Africa) genotype was the most prevalent genotype found in Indonesia, Thailand, Malaysia, and Singapore, whereas during 2007–2014, the Asian genotype was most prevalent in Indonesia and the Philippines (Wahid *et al*., 2017). The fact that the ECSA genotype was found in Asia is because it is believed that a point mutation in the virus E1 glycoprotein has increased the infectivity of *Ae. albopictus* mosquito species. This genetic change (E1-A226V) likely contributed to the magnitude and distribution of outbreaks (Staples *et al*., 2009).

In 2007, the first autochthonous CHIKV outbreak was reported in Emilia-Romagna, Italy. The vector of CHIKV (*Ae. albopictus*) is present in almost 20 European countries and the ECSA genotype was responsible for the emergence of CHIKV in Europe. More than 200 cases of CHIKV were confirmed between July and September 2007. Furthermore, France reported significant numbers of laboratory-confirmed autochthonous cases in 2010, 2013, and 2014 (Wahida *et al*., 2017). In Spain, the risk of autochthonous transmission of the virus has increased in recent years due to the high number of travelers returning to Spain from countries affected by the 2013 Chikungunya epidemic in the Caribbean and South America. In addition, the vector *Ae. albopictus* is established in some areas of Spain (Catalonia, Valencia, Murcia, Andalusia, the Basque Country and the Balearic Islands). Between 2008 and 2014, 264 imported cases of Chikungunya were confirmed in Spain, mainly from the Caribbean and

Indian Ocean, of which 234 were confirmed in 2014. However, no case of autochthonous transmission has occurred yet (Fernández-García *et al*., 2016).

In the American continent, Asian lineage of the CHIKV was initially identified on Saint Martin Island in October 2013, and from there the virus rapidly spread to several countries and territories. From the onset of the outbreak to early August 2016, autochthonous transmission of the virus has been confirmed in 48 countries or territories in the Caribbean, Central America, South America and North America, with more than 1 million suspected cases (Burt *et al*., 2017). The spread and establishment of the virus in new endemic regions is likely to be dependent on the availability of competent vectors.

Currently, chikungunya fever has been identified in nearly 40 countries, and in 2008 it was listed as a US National Institute of Allergy and Infectious Diseases (NIAID) category C priority pathogen (Schwartz and Albert, 2010).

### 1.3 Genome organization and molecular structure of the Chikungunya virus

CHIKV is a virus of the alphavirus genus and belongs to the *Togaviridae* family. CHIKV has three genotypes: Asian, West African and East Central South African, according to their geographical distributions.

The virus itself is a positive-sense single-stranded RNA virus of approximately 11.8 kb length. It has an icosahedral capsid that is covered by a lipid layer, a diameter of approximately 65 nm, and is sensitive to temperatures above 58 °C (Ganesan *et al*., 2017). Regarding its genome (figure 3), it contains two open reading frames (ORF), one at the 5 ’end and the other at the 3’ end. The ORF at the 5 ’end produces four non-structural proteins related to the replication complex of the virus (nsP 1-4) and the ORF at the 3’ end produces the structural proteins, which are composed of a capsid protein (CP), two envelope glycoproteins (E1 and E2) and 2 small cleavage products (An *et al*., 2017).

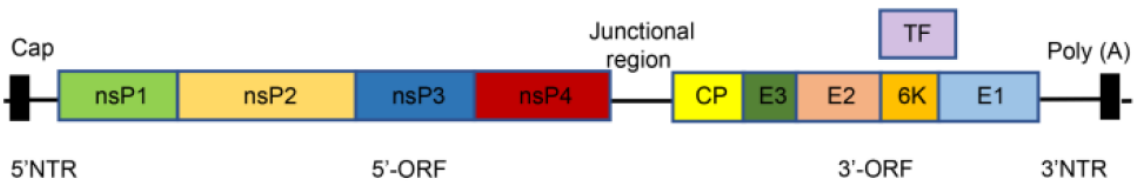


**Figure 3**. Genome structure of the Chikungunya virus (An et al., 2017).

### 1.4 Pathogenesis

CHIKV is injected into blood capillaries and dermis after the bite of the mosquito. In this first intradermal stage, CHIKV infects the most common cells of connective tissues, epithelial cells and intradermal fibroblasts. These cells are susceptible to viral production and hence viruses enter the blood vessels. Subsequently, CHIKV reaches high levels in the blood circulation during the acute phase, where it is also possible to detect it *in vivo* in the monocytes (Rougeron *et al*., 2015). Furthermore, it is believed that monocytes are responsible for the viral spread to different tissues and organs and systemic infection. Afterwards, the virus spreads through the muscles, joints and liver mainly through the blood (Schwartz and Albert., 2010) and finally, the macrophages and stromal cells of the spleen and lymph nodes are also infected and, together with the tissues of the joints, can be sites of persistence of the virus (Rougeron *et al*., 2015).

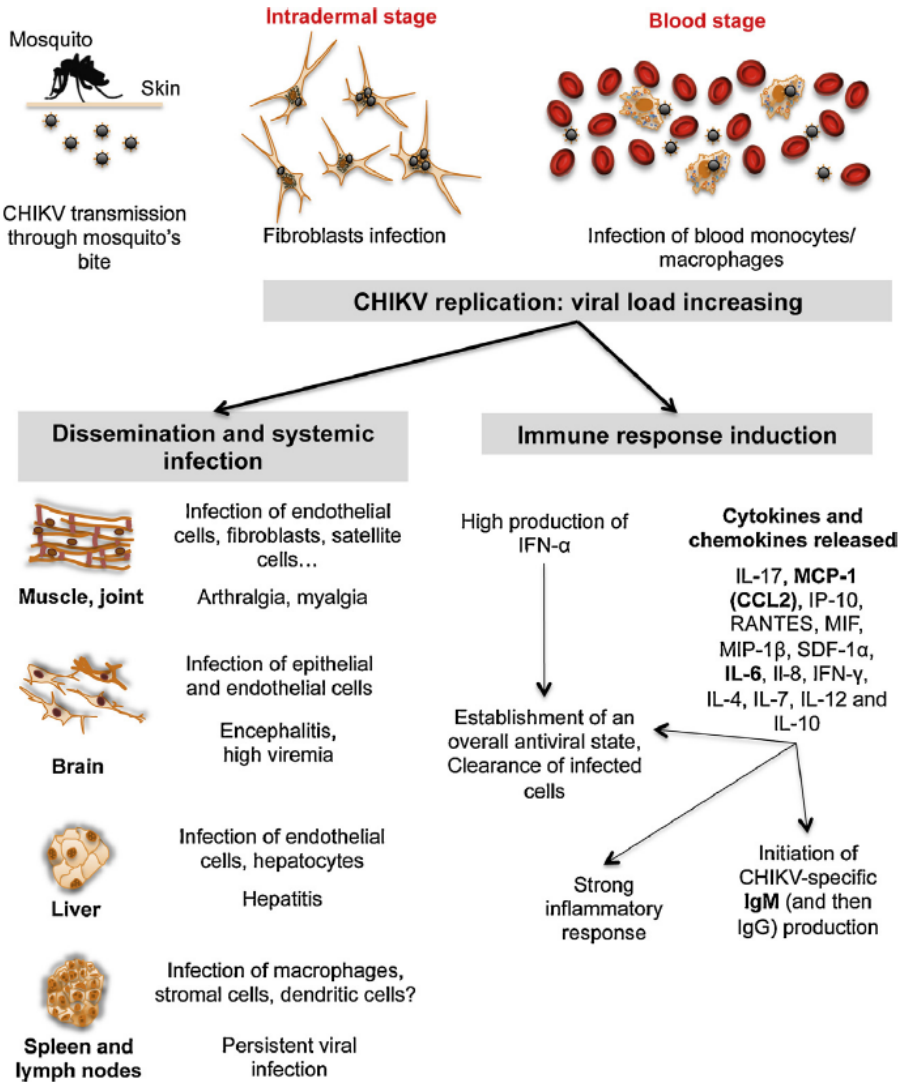


**Figure 4.** Model of viral infection by chikungunya virus (Rougeron *et al*., 2015).

When viral infection begins, innate immunity is activated and there is an elevated production of proinflammatory cytokines, chemokines, and growth factors such as IL-6, MCP-1, IP-10 and RANTES (Rougeron *et al*., 2015). IFN-α/β play an important role in controlling and eliminating the infection by producing antiviral proteins. It has also been shown that a high level of IFN-α is associated with rapid control of viremia (An *et al*., 2017).

The $CD8^+$ T lymphocytes are activated during the acute phase and contribute to the control of the replication of the virus; however, the $CD4^+$ T lymphocytes are activated at the end of the acute phase to facilitate the humoral response. The number of activated T cells is increased especially in patients with persistent CHIKV-induced arthritis and is believed to play an important role in the pathogenesis. Patients infected with CHIKV develop a robust antibody response, with detectable IgM levels within a few days of infection and neutralizing IgG anti-CHIKV antibodies typically measurable in the second week of infection (Burt *et al*., 2017). Further, the specific antibodies produced by the B lymphocytes are directed to the B domain of the E2 protein of CHIKV (An *et al*., 2017). In addition to T and B cells, it is likely that other multiple cell types play a role during infection such as natural killer cells. A greater number of them have been found in the peripheral blood of patients with persistent CHIKV-induced arthritis than in healthy controls.

### 1.5 Symptoms

Those patients infected by CHIKV can experience up to three different phases of the disease. First, the acute phase occurs in the first 3 weeks with an incubation period of 4-7 days. This phase is mainly characterized by acute fever (39-40 °C) that can progress to severe, macropapular rash and inflammatory arthralgia (Burt *et al*., 2017). Gastro-intestinal and neurological complications may also occur during this phase (Schwartz and Albert, 2010). From the fourth week to three months after the post-acute stage, it is characterized by continued severe arthritis and synovial inflammation (An *et al*., 2017). Finally, after three months the chronic phase takes place, which occurs when the symptoms still persist. Approximately 50-60% of individuals infected with CHIKV can progress to the chronic phase, with symmetric peripheral polyarthralgia and polyarthritis for years, during which no viremia is detected, but may contain viral reservoirs in satellite muscle cells and synovial macrophages. When the disease is chronic, it has a substantial repercussion on the quality of life of patients and a considerable economic impact in epidemic areas (An *et al*., 2017). The

mechanism of the disease is not yet fully understood, and the development of drugs and vaccines is necessary. It should be noted that, during the acute phase, the viral load can reach $10^8$ viral particles per ml of blood, and the plasma concentration of type I interferons (IFNs) is in the range of 0.5-2 ng per ml, accompanied by a robust induction of other pro-inflammatory cytokines and chemokines (Schwartz and Albert, 2010).

### 1.6 CHIKV infection models

Animal and *in vitro* models are essential to understand the pathogenesis of the virus and develop effective treatments against the disease. Different animal models and *in vitro* studies have shown that CHIKV infects multiple cell types, including dendritic cells, macrophages, sinovial fibroblasts, endothelial cells and myocytes.

*In vitro* culture systems are the easiest and cheapest way to create a CHIKV infection model. In these cultures, a wide variety of cells are used in order to assess the total extent of the disease, including primary human skeletal muscle myoblasts, human blood monocytes, human primary fibroblast synoviocytes, and human osteoblasts, given the known tropism of CHIKV chronic for bones and synovial tissues (Ganesan *et al*., 2017). However, although *in vitro* model has shown some progress in accurately modeling the course of the disease, it still cannot accurately predict *in vivo* behavior.

Nonhuman primates are particularly relevant for studies of pathogenesis and assessment of therapies because their physiology and immune system are similar to those in humans and they are also natural hosts of CHIKV. An experiment was conducted with adult cynomolgus macaques inoculated intradermally (ID) and intravenously (IV) with a strain of CHIKV obtained from an infected patient during the outbreak of Chikungunya on La Réunion Island (Cirimotich *et al*., 2017). The monkeys developed symptoms similar to those observed in humans; high fever, skin rashes and gingival bleeding. All IV or ID infected animals showed substantial and significant monocytopenia, lymphopenia, granulocytosis and thrombocytopenia in serum and these changes were associated with peak viremia (2-4 DPI). In addition, during the viremia peak CHIKV also revealed a marked tropism for spleen, lymph nodes, and liver. It should be noted that extensive infiltration with macrophages was observed in lymphoid tissues and liver in all animals. These infiltrates appeared early in infection and in many cases persisted for at least 6 months after virus inoculation. This long-term

persistence of CHIKV is because macrophages act as cellular reservoirs during the later stages of CHIKV infection in vivo (Labadie *et al*., 2010). This persistence of CHIKV over extended periods could explain the long-lasting symptoms, in particular arthralgia, observed in humans. Another comparative study with cynomolgus macaques inoculated with CHIKV intradermally and by aerosols showed that it is also possible the transmition of the virus through exposure to aerosols (Cirimotich *et al*., 2017), however, this exposed animals developed milder symptoms and low levels of viremia.

Rodent models are widely used to create models of infectious diseases *in vivo*, therefore, they may be more useful for understanding the pathophysiology of the Chikungunya disease. It has been discovered that type-I IFN signaling plays a critical role in the control of the infection and is associated with severe infection when it is deficient. This fact has been demonstrated in a study that used IFN-α/βR mice knock out with one or two copies of IFN-α/β receptor null allele (Couderc *et al*., 2008). It was found that when they were deficient in IFN null allele the virus spreads abundantly in the liver, muscles, joints, skin and brain at 3 days after virus inoculation. In addition, mice had high viral titers in liver, spleen and serum. However, in WT (wild type) or IFN-α/$\beta R^{+/-}$ mice, IFN was able to control the infection at a dose-effect level. It was also observed that neonatal WT mice inoculated with the virus were vulnerable and died within a few days, whereas adult WT mice were resistant to CHIKV.

In terms of cellular tropism, in IFN-α/$\beta R^{-/-}$ mice, CHIKV antigens were found in the liver in endothelial cells of the sinusoids, in mature macrophages and a small number of viral particles in Kupffer cells (macrophages located in the liver). In the skeletal muscles of IFN-α/$\beta R^{-/-}$ and IFN-α/$\beta R^{+/-}$ mice, the predominant immunolabeling was found in the connective tissue, especially in the epimisium and in lesser amount in the perimisium and endomysium and in addition, the main target cells of the muscle were the fibroblasts. Immunolabeling was also observed in the connective tissue fibroblasts of the joint located under the synovial wall, however, the bone and cartilage tissues were not infected. Furthermore, it was also observed in the fibroblasts of the deep dermis. IFN-α/$\beta R^{+/-}$ mice presented this same staining but in smaller amounts. The tropism of viral cells in infected peripheral tissues of neonates, including muscles, joints and skin, was similar to that of adult mice, with a pronounced tropism for fibroblasts (Couderc *et al*., 2008). A notable difference was the presence of severe necrotic myositis consistent with severe myofiber necrosis, and inflammation manifested by infiltration of lymphocytes and monocytes/macrophages. Regarding the central nervous system, there was severe vacuolization in the epithelial cells of the choroid plexuses and

sometimes in the adjacent ependymocytes. The choroid plexuses, the ependymal wall and the leptomeningeal cells presented immunolabeling. However, microglial cells and astrocytes were not immunolabeled. In the CNS of infected WT mouse neonates (Couderc *et al*., 2008), CHIKV infection was only detected in the leptomeninges.

Another comparative study between neonatal and 14 days-old mice (ICR and CD-1 strains), infected by CHIKV strain (LR 2006-OPY1) isolated from a patient infected by the Reunion outbreak in 2006, obtained results on histopathology (Ziegler *et al*., 2008). In neonatal mice at 3 DPI there were a few foci of hepatocytes necrosis in the parenchyma without specific zonal distribution. From 2-4 DPI they showed mild atrophy of focal muscle bundles and from 5 DPI they showed muscle necrosis and a little mononuclear inflammatory cellular infiltration. There was also a strong lymphocytic necrosis in the lymph nodes. In the newborn mice, their limbs showed extensive multifocal myositis with necrosis. In addition, the skin exhibited extensive necrosis in the subcutaneous muscle, with calcification and similar dystrophic calcifications were also present in the joint cartilage. Pathological lesions in skeletal muscle were also observed in young mice but were less severe than in neonatal mice.

In this project, a study of the CHIKV pathogenesis has been performed in mice infected by two strains of CHIKV (S27 (EA226) and ITA1 (E1A226V)) from an experiment already carried out at CReSA under Biosecurity Level Containment 3. The objective of the present study is to better characterize the tropism of the CHIKV by immunohistochemistry. Additionally, a semiquantification of the immunolabeling was performed to compare both CHIKV strains in this mice model. Thus, it improves the understanding of how the virus behaves when it infects animals and it will help in testing new antivirals for human treatment.

## 2. Materials and methods

### 2.1 Viral strains

Two CHIKV strains of the ECSA lineage were used: S27 Petersfield and ITA1 TAM E1, named S27 and ITA hereafter respectively. S27 has an alanine in the position 226 of the E1 glicoprotein (E1-226A), whereas ITA has a valine in the same position (E1-226V). The strain S27, (GenBank AF369024), was isolated from a febrile patient during the 1952 Tanzania outbreak. It was kindly provided by the Department of Arboviruses and Imported Viral Diseases of the National Centre for Microbiology at Institute of Health Carlos III (ISCIII),

Madrid, Spain. The ITA strain (GenBank EU188924.2) was isolated from an autochthonous human case in Italy (2007). It was kindly provided by the Lazzaro Spallanzani National Institute for Infectious Diseases (INMI), Rome, Italy. Viral stocks were previously produced on Vero cells (African green monkey kidney cell line) and were stored at -80ºC prior to their use in mice experimental infections.

### 2.2 Mice experimental CHIKV infection

In 2013, a mice experimental CHIKV infection was performed in A129 knockout mice for interferon $\alpha/\beta^{(-/-)}$ receptor, using two strains of S27 and ITA1 virus. A total of 67 8-weeks old mice (males and females) were distributed in seven groups randomly. For inoculation, the animals were anesthetized with isoflurane (4%) and inoculated with a syringe subcutaneously in abdominal area with the virus corresponding to the following doses: $10^2$ $TCDI_{50}$, $10^4$ $TCDI_{50}$ and $10^6$ $TCDI_{50}$, in a final volume of 100 µl. The control animals received 100 µL of PBS saline. In the original experiment, the viral load in mouse tissues was also studied, in which positivity was observed in liver, spleen, encephalon, inguinal lymph node and calf.

**Table 1.** Original experiment. Total number of infected mice for each strain at different doses ($10^2$ $TCDI_{50}$, $10^4$ $TCDI_{50}$ and $10^6$ $TCDI_{50}$), and different days post-infection (2 DPI, 3DPI, 4DPI) that were euthanatized and sampled for histopathology. The remaining animals died from the viral infection and were not sampled for histopathological analysis.

| **S27** | **$10^2$ n=10** | **$10^4$ n=12** | **$10^6$ n=10** | **ITA1** | **$10^2$ n=10** | **$10^4$ n=12** | **$10^6$ n=10** | **Control (PBS) n=3** |
|---|---|---|---|---|---|---|---|---|
| **2 DPI** | 1 | 1 | 3* | **2 DPI** | -- | 1 | 1* | 3* |
| **3 DPI** | -- | -- | -- | **3 DPI** | 4 | 3 | 3*+ 1 | |
| **4 DPI** | -- | -- | -- | **4 DPI** | 1 | -- | -- | |

(*) Animals selected for the immunohistochemical study.

Table 1 shows all the animals that were euthanized and sampled for histopathological studies, the other mice died spontaneously due to the viral infection, and therefore, they were not sampled for histopathology to avoid autolysis artifacts and epitope degradation. For this immunohistochemical study, a total of 7 infected animals were selected at a dose of $10^6$ $TCDI_{50}$ (3 for S27 strain at 2DPI and for ITA1 one at 2DPI and 3 at 3DPI); along with 3 mock-infected controls. The animals were perfused through the intracardiac route with PBS to minimize the amount of blood in the tissues and the following samples were collected: liver, spleen, gastrocnemius muscle, encephalon, inguinal lymph node, skin and joint (knee and foot).

### 2.3 Tissue processing

The collected samples were fixed in formaldehyde and then introduced into the tissue processor (Leica TP1020) for paraffin embedding, which follows this procedure overnight: formaldehyde 1 (1h), formaldehyde 2 (1h), ethanol I 80º (1h), ethanol 96º I (1h), ethanol II 96º (1h), ethanol I 100º (1h), ethanol II 100º(1h), Xylol I (1h), xylol II (1h), paraffin I (1h), paraffin II (1h) , paraffin III (1h). After that, the samples were included in cassettes to form paraffin blocks in the paraffin station. The samples collected were included in paraffin blocks, then cut with the microtome (microtome Leica RM 2255) at 4 micrometer thick sections and placed in silane treated glass slides.

The sections were stained with hematoxilin-eosin in order to visualize the lesions produced in the tissues.

### 2.4 Immunohistochemistry

Subsequent sections of the samples were dewaxed and hydrated in an automatic dyer (Leica AutoStainer XL) which follows this procedure: xilol I (5 min), xilol II (5 min), ethanol 100º (5 min), etanol 96º (5 min), etanol 80º (5 min), etanol 50º (5 min) and after that, the samples were washed with distilled water for 5 minutes and the endogenous peroxidase was blocked. This blocking step is necessary so that the 3-3' diaminobenzidine (DAB) chromogen does not bind to endogenous peroxidases that may be present in the tissues. To carry it out, the samples were included in a solution of methanol and 3% hydrogen peroxide under agitated conditions for 30 minutes and at room temperature. Finally, samples were washed with distilled water and PBS buffer for 5 minutes. To ensure that the primary antibody binds to the antigens, an antigenic retrieval step was taken a 0.1 % protease solution + PBS buffer was used, then washed with distilled water for 5 minutes and later with PBS-tween20 three times for 5 minutes. Finally, a solution of PBS-tween20 + bovine serum albumin (BSA) at 2% was used to block samples from non-specific binding and incubated at room temperature for 2 hours.

The samples were incubated overnight at 4ºC with a dilution (1/500) of polyclonal primary antibody created in rabbit against the capsid protein of CHIKV. Then, the samples were warmed at room temperature for 20 minutes and washed 5 times with PBS-Tween 20 for 5 minutes. Once concluded, incubation with a secondary anti-rabbit antibody (Envision + system-HRP labelled Polymer Anti-Rabbit (Dako)) was carried out at room temperature for 45 minutes. Subsequently, 3 washes were made using PBS for 5 minutes.

The visualization of the reaction was carried out with a 0.05 % DAB solution as a chromogen at room temperature under agitated conditions (200 ml PBS + 0.1 g DAB + 100

microliters hydrogen peroxide). Then, they were washed with distilled water for 5 minutes and contrasted with Hematoxylin.

Finally the samples were dehydrated and rinsed with xylene in an automatic dyer (Program 4, Leica AutoStainer XL) and proceeded to the final assembly with a mixture of distyrene, a plasticizer (tricresyl phosphate) and xylene in an automatic assembler (Automatic coverslip assembler Leica CV 5030).

### 2.4.1 Result interpretation

Those mouse tissues stained brown means that the virus is found there, because the primary antibody has been bound to the capsid proteins. Afterwards, the secondary antibody and the DAB chromogen allowed to amplify the signal and to stain the tissue. Therefore, it was interpreted as positive tissue to the virus. However, whenever a staining patterns was also found in the control animal tissues it was interpreted as artefactual staining and was not taken into account in the results.

### 2.4.2 CHIKV antigen semiquantification in tissues

The stained samples were observed under the optical microscope (Nikon Eclipse 50i) and a value was assigned to certain cell type of each tissue according to the amount of labeling observed (0: no cells stained, 1: very few cells stained, 2: some cells stained, 3: many cells stained, 4: all cells stained).

The Mann Whitney U test for non-parametric variables was applied (*P <0.05 with a 95% confidence interval), to establish whether the differences between the two strains were statistically significant or not.

## 3. Results and discussion

In the original experiment, the lesions in each organ infected by both strains were evaluated, both at 2 DPI and 3 DPI. However, no 4 DPI could be evaluated because almost no animal survived the following days. Most of the mice that survived until they were euthanized (2 DPI, 3 DPI) showed lympholysis in the spleen and in the lymph node. There were also observed mild or moderate lipidosis in the liver in both samples infected with S27 and ITA1 strains, however, in the ITA1 strain, focal areas of hepatocyte necrosis was observed in both infected with $10^2$ $TCDI_{50}$ and $10^4$ $TCDI_{50}$. On the other hand, no evidence of arthritis, myositis or encephalitis was found in any mice.

In the present study, an inmunohistochemistry technique was performed to find out where the virus was in the tissues studied and relate it to the lesions found. As mentioned in materials and methods section, the following samples were studied: liver, spleen, gastrocnemius muscle, encephalon, inguinal lymph node, skin and joint (knee and foot) and the virus specific inmunolabeling is described.

## 3.1 Virus antigen immunolabeling in the sampled tissues

### 3.1.1 Liver

In mice livers infected with both strains S27 and ITA1, staining was observed in some endothelial cells of the portal vein and hepatic sinusoids, as well as in fibrocytes of the blood vessel's basal lamina (Figures 5A and 5B). The inmunolabeling in the hepatic sinusoids and in the portal veins were not constant and only some immunolabeled foci were found. This makes sense because once the virus is introduced into the host organism, it replicates and disseminates primarily to the liver through the blood, as seen earlier in studies about the pathogenesis of the virus (Rougeron *et al*., 2015). In control mice no staining was observed (Figure 5C).

A population of immunostained cells were observed, with smaller nuclei than hepatocyes and sometimes with conspicuous ramifications. They have been interpreted as kupffer cells, because they showed the characteristic shape of macrophages. Additionally, they were distributed in a non-constant way and the amount was moderate.

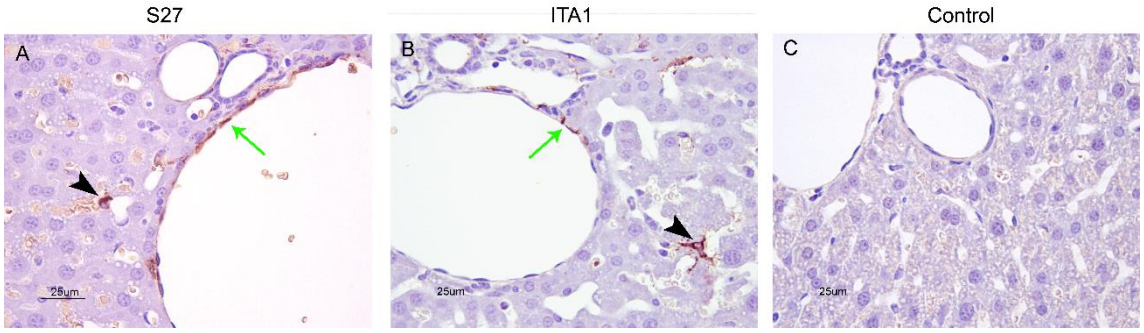


**Figure 5**. Liver tissue of mice infected with $10^6$ pfu of CHIKV and control mice (25 µm). (A) Mouse liver infected with S27 strain 2DPI. Immunolabeled endothelial cells of the portal vein (green arrow) and Kupffer cell were clearly observed (arrowhead). Hepatocytes, the artery and the bile duct of the portal space were not stained. (B) Mouse liver infected with ITA1 strain 3DPI. The stained upper part is a hepatic sinusoid, and there is also a Kupffer cell (arrowhead). Additionally, there are some endothelial stained cells in the portal vein (green arrow). The artery and the bile duct are not stained. (C) Control liver without staining.

Intracytoplasmatic inclusion were observed in hepatocytes of mice infected with the ITA1 strain but not in controls with the IHQ protocol used, however, during the set-up of the technique these inclusions were also observed in control animals, thus it was concluded that it consisted of non-specific staining (see figure 25A, 25B and 25C in artifacts section).

Semiquantification of the amount of immunolabeling in each cell type was performed in order to compare the two studied CHIKV strains. In general, the staining was found in a greater quantity in those livers infected with S27. However, the differences between both strains were not statistically significant, but S27 seemed to be a bit more aggressive (figure 6).

The results observed in the liver confirm the marked tropism of the virus for the endothelial and Kupffer cells. This has also been concluded previously (Couderc *et al*., 2008), which support the results observed in the mice livers of the present study. This tropism for the liver has also been confirmed in experiments with non-human primates, however in this cases there was a high infiltration of macrophages (Labadie *et al*., 2010).

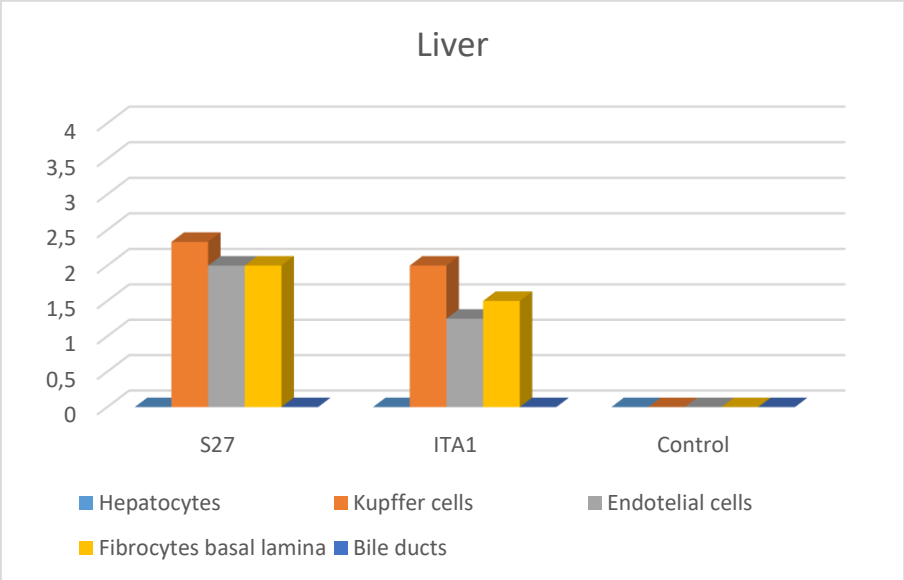


**Figure 6.** Comparative plot of CHIKV S27 and ITA1 strains in mice liver. The values are assigned according to the number of stained cells; 0, no cells stained; 1, very few cells stained; 2, some cells stained; 3, many cells stained; 4, all cells are stained. The values obtained in the plot are the mean of all the values assigned in each liver of both strains. The differences between both strains were not statistically significant in Kupffer cells (P=0.59), endothelial cells (P=0.15) and fibrocytes (P=0.37).

### 3.1.2 Spleen

The mice spleens infected with S27 strain showed a high amount of macrophages and some stained lymphocytes of the white pulp (figure 7A), whereas those spleens infected with the ITA1 strain seemed to have a smaller quantity of these stained cells. Regarding fibrocytes, a few of them were found immunolabeled in both strains, but it seemed there were more stained fibrocytes in those spleens infected by the ITA1 strain. However in S27 strain most of them were found in the spleen trabeculae (figure 7D), whereas in strain ITA1 there were none (figure 7E). In the ITA1 strain they were observed in the basal lamina under the endothelial cells of the blood vessels. Furthermore, there were very few marked endothelial cells in both strains and few immunolabeled megakaryocytes were also found in the subcapsular portion of the organ. The differences between infected (figures 7A, 7B, 7D and 7E) and control spleens (figures 7C and 7F) were not statistically significant (figure 8).

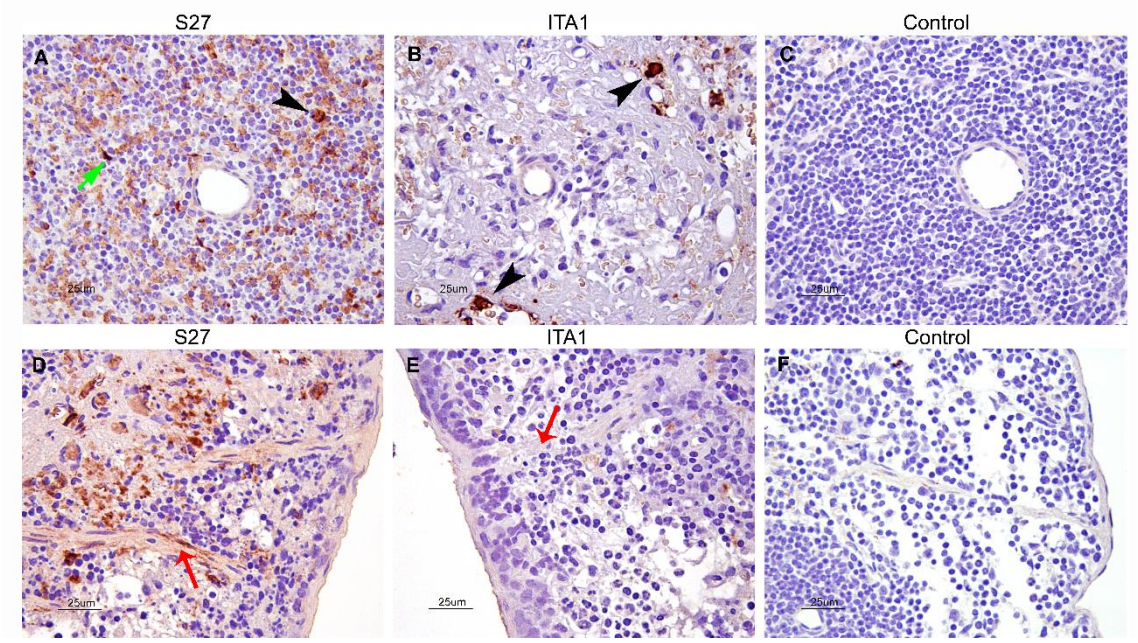


**Figure 7.** Spleen tissue of mice infected with $10^6$ pfu of CHIKV and control mice (25 µm). (A) White pulp of a spleen infected with S27 strain 2DPI. Some stained macrophages (arrowhead) were surrounding the artery and also multiple lymphocytes could be observed (green arrow). (B) White pulp of a spleen infected with ITA1 strain 3DPI. Immunolabeled macrophages could be observed (arrowheads). It could be noted a remarkable lymphoid depletion compared to 7C. (C) Control spleen without immunostaining. (D) Positive trabeculae (red arrow) of a S27 infected spleen. (E) Unstained trabeculae (red arrow) of an ITA1 infected spleen. (F) Control spleen without staining.

Besides, there was a great cellular tropism of the virus towards a sort of cells that have been interpreted as macrophages. This tropism been observed in non-human primates models (Labadie *et al*., 2010), where an extensive infiltration of macrophages occurs and it makes

the virus persist longer in lymphoid tissues. CHIKV studies in humans have shown infected macrophages in the spleen as well (Rougeron *et al*., 2015).

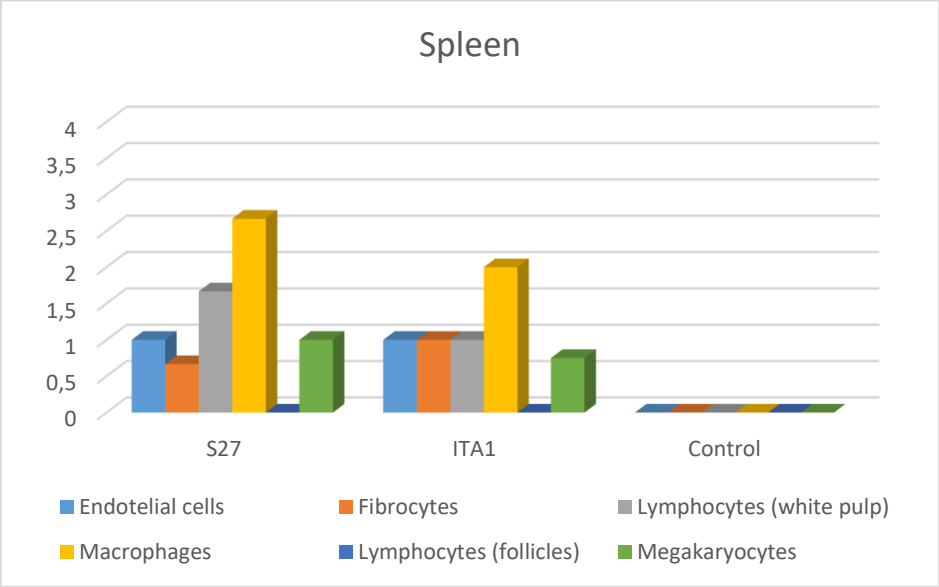


**Figure 8.** Comparative plot of CHIKV S27 and ITA1 strains in mice spleen. The values are assigned according to the number of stained cells; 0, no cells stained; 1, very few cells stained; 2, some cells stained; 3, many cells stained; 4, all cells are stained. The values obtained in the plot are the average of all the values assigned in each spleen of both strains. More stained macrophages and lymphocytes were observed in spleens infected with S27 strain than those infected with ITA1. In neither of the two strains was observed staining in the lymphocytes of the follicles. The differences between both strains were not statistically significant in endothelial cells (P=1), fibrocytes (P=0.72), lymphocytes of the white pulp (P=0.37), macrophages (P=0.21) and megakaryocytes (P=0.72). The cells of the control spleens did not present staining.

### 3.1.3 Lymph node

The mice lymph nodes infected with both strains showed immunolabeled macrophages in the outer parts of the tissue, some lymphocytes and fibrocytes of the capsule (Figures 9A, 9B, 9D and 9E). A greater number of these cells was observed in those lymph nodes infected with the S27 strain, however, the differences between both strains were not statistically significant (figure 10). The reason that the macrophages were at the outer parts of the lymph node may be due to the fact that they had been recently infiltrated into the organ caused by the viral infection, and therefore, contribute to its control. In non-human primates models (Labadie *et al*., 2010), was confirmed the tropism for the virus in the lymph nodes because a high infiltration of macrophages was observed. CHIKV studies in human also have shown tropism for the lymph nodes (Rougeron *et al*., 2015).

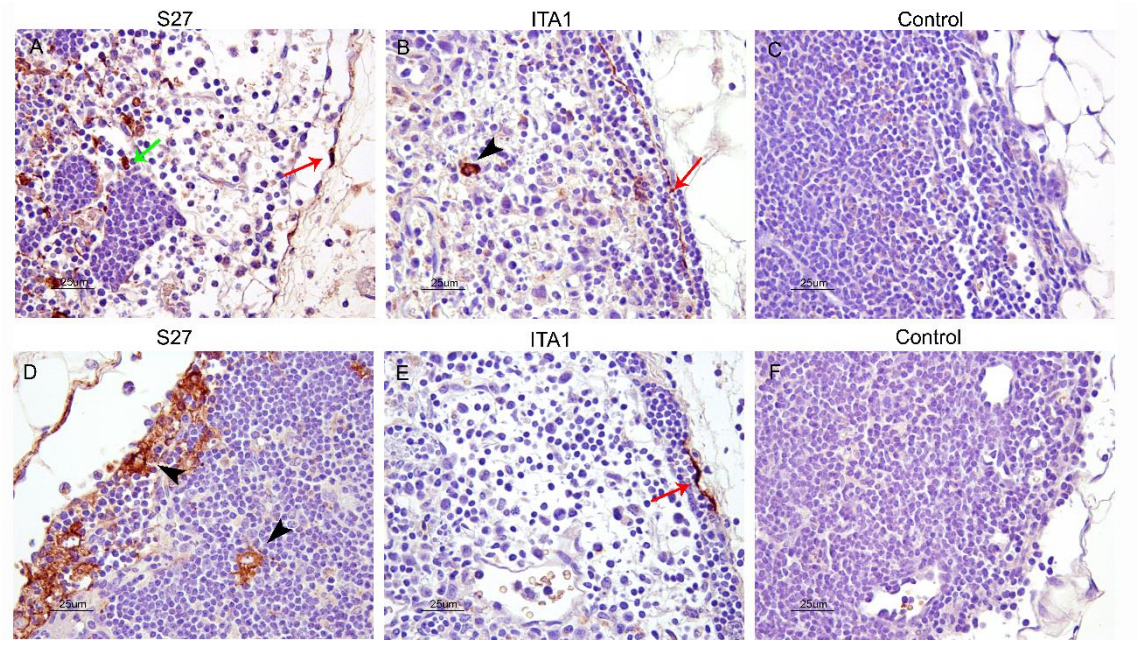


**Figure 9.** Lymph node tissue of mice infected with $10^6$ pfu of CHIKV and control mice (25 µm). (A) Lymph node of a mouse infected with S27 strain 2DPI. Some stained macrophages and lymphocytes are oberved (arrowsheads) and also multiple positive fibrocytes of the capsule (red arrows). (B) Lymph node of a mouse infected with ITA1 strain 3DPI. A macrophage and multiple fibrocytes are stained. It should be noted lymphoid depletion is more evident in this animal. (C) Control lymph node without staining. (D) Positive fibrocytes and a macrophage (arrows) of a S27 infected lymph node. (E) Some stained fibrocytes of the capsule are observed and also lymphoid depletion. (F) Control lymph node without staining.

A remarkable lympholysis was observed in the lymph nodes infected with the ITA1 strain (Figures 9B and 9E), which can be clearly differentiated compared to the control lymph nodes (Figures 9C and 9F). In addition, greater lysis was observed in those mice infected with ITA1 and which died at 3 DPI.

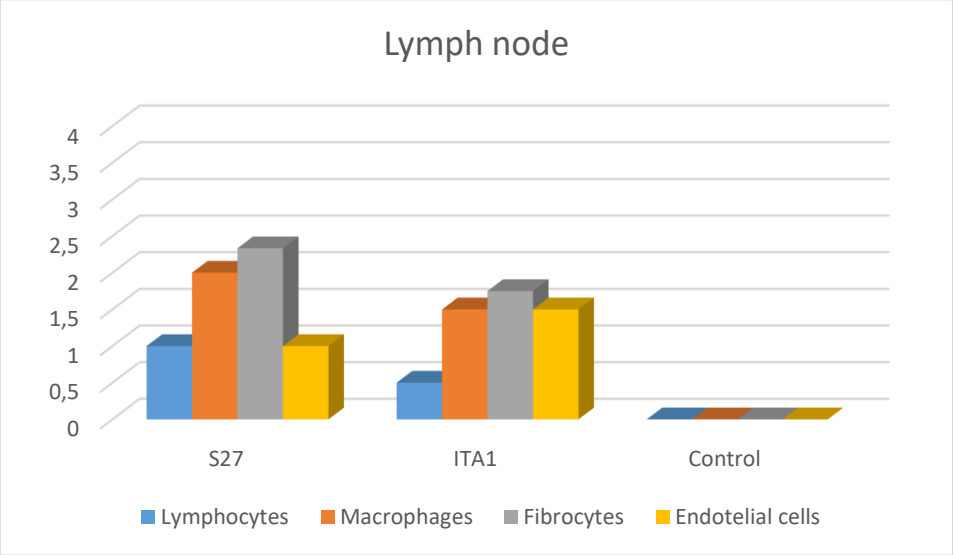


**Figure 10.** Comparative plot of CHIKV S27 and ITA1 strains in mice spleen. The values are assigned according to the number of stained cells; 0, no cells stained; 1, very few cells stained; 2, some cells stained; 3, many cells stained; 4, all

cells are stained. The values obtained in the plot are the average of all the values assigned in each lymph node of both strains. More stained macrophages, lymphocytes and fibrocytes were observed in lymph nodes infected with S27 strain than those infected with ITA1. The differences between both strains were not statistically significant in lymphocytes (P=0.37), macrophages (P=0.15), fibrocytes (P=0.47) and endothelial cells (P=0.59). The cells of the control lymph nodes did not present staining.

### 3.1.4 Skeletal muscle

In the mice skeletal muscles, non-specific staining of the muscle fibers was observed, as it was found in both control and infected mice (See figures 23A, 23B and 23C in artifacts section). Therefore, it was not taken into account in the evaluation of the results. This non-specific staining was also observed in the axons of the nerve sheath in both control (figure 11F) and infected mice (figures 11D and 11E).

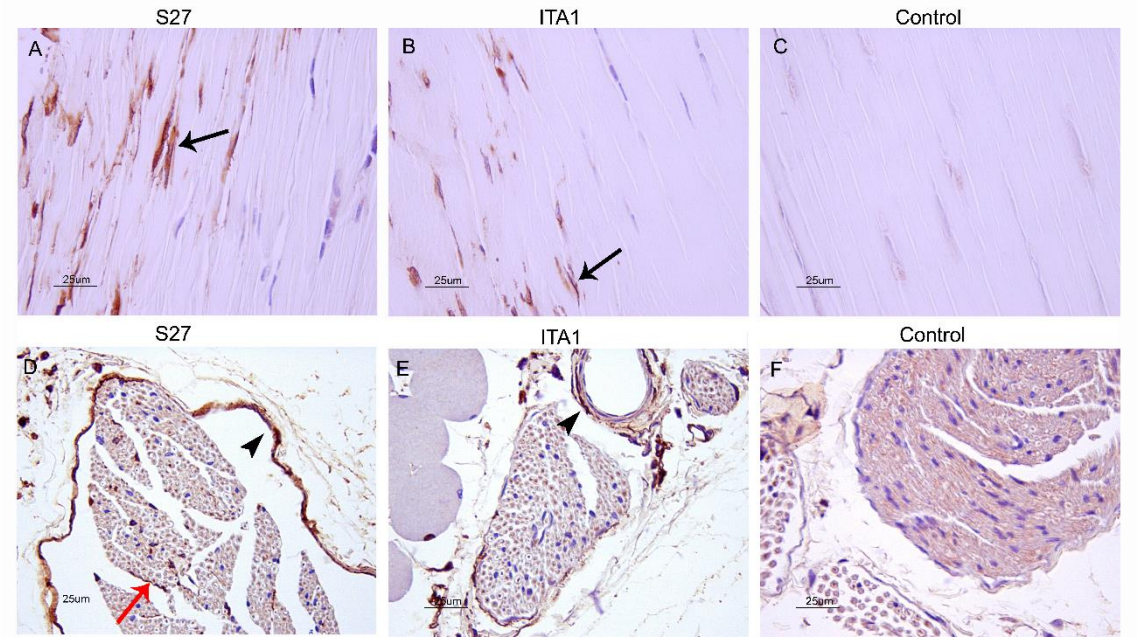


**Figure 11.** Tendon and nerve sheath tissue of mice infected with $10^6$ pfu of CHIKV and control mice (25 µm). (A) Tendon of a mouse infected with S27 strain 2DPI. Some stained tenocytes are oberved (arrow). (B) Tendon of a mouse infected with ITA1 strain 3DPI. Some tenocytes are stained (arrow). (C) Control tendon without staining. (D) Positive fibrocytes of the epineurium (arrowhead) of a S27 infected muscular nerve sheath. Besides it can be seen some parts of the nerve sheath stained, it could be peri/endoneurium or Schwann cells (red arrow), it cannot be confirmed with the techniques used here. (E) Some stained fibrocytes of the basal lamina, below the artery are observed (arrowhead). (F) Control nerve sheath with non-specific stained axons.

Regarding specific stains, it could be observed in some tenocytes on the tendons in both infected mice with S27 and ITA1 (figures 11A and 11B) compared to the control (figure 11C). In terms of the peripheral nerve sheath, many fibrocytes were stained in the epineurium

and also some fibrocytes on the basal lamina of the blood vessels (figures 11D and 11E). These stained fibrocytes were not observed in control mice (figure 11F). However, in those muscles infected by the S27 strain, small cells were immunolabelled among the nerve fibers. These could be fibrocytes forming epi/endoneurium or Schwann cells lining the nerve fibers. It cannot be ensured what cell type it may be by using the immunohistochemical technique of this study. It is not possible to differentiate them, therefore, we cannot discard either of these two options (figure 11F).

More tenocytes and stained fibrocytes of the nerve sheath were observed in muscles infected with the S27 strain than in those infected with ITA1 strain, but a greater number of stained endothelial cells were observed in muscles with ITA1. However, the differences between both strains were not statistically significant (Figure 13). The overall staining of endothelial cells was moderate, suggesting the spread of the virus to the muscles through the blood vessels.

It should be noted that few fibrocytes in small parts of the endo and perimysium were stained in both mice infected with S27 and ITA1 strains (figures 12A and 12B), but it were not in control mice (figure 12C).

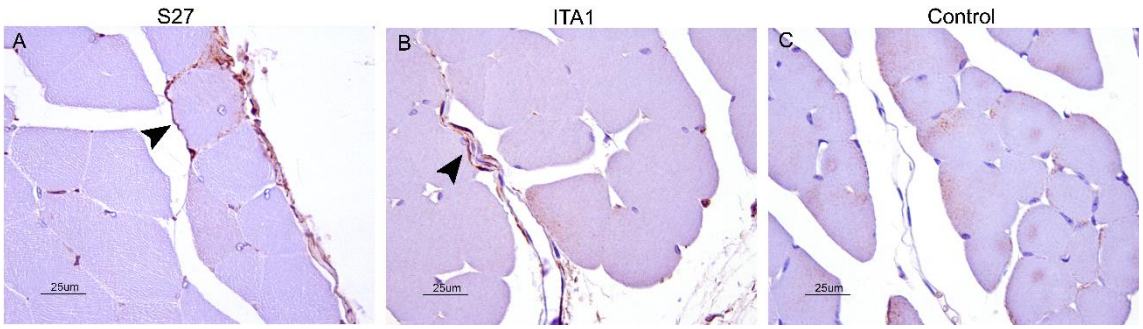


**Figure 12.** Endo and perimysium stained of mice infected with $10^6$ pfu of CHIKV and control mice (25 µm). (A) Endo and perimysium of a mouse infected with S27 strain 2DPI (arrowhead). (B) Endo and Perimysium of a mice infected with ITA1 strain 3 DPI (arrowhead). (C) Control skeletal muscle with unstained endo and perimysium.

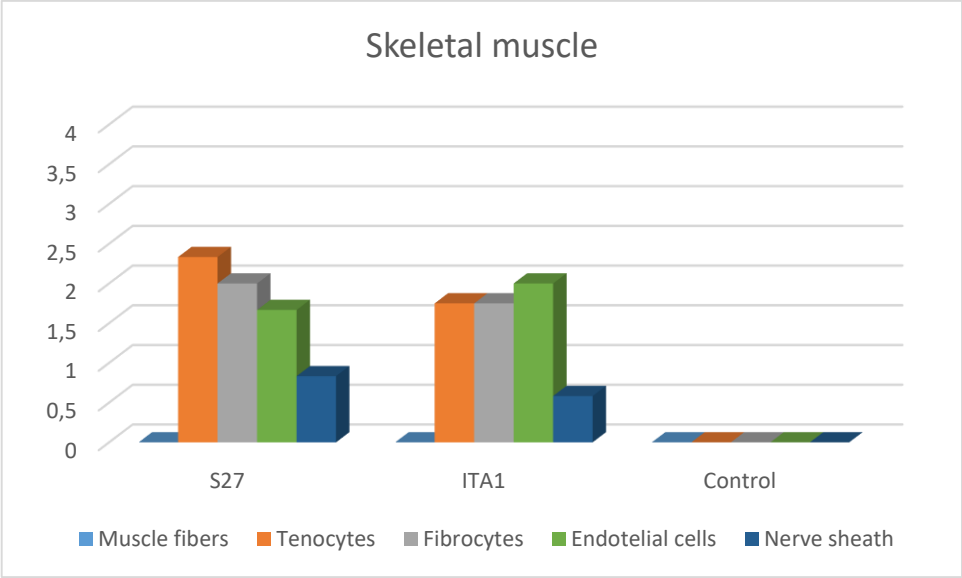


**Figure 13.** Comparative plot of CHIKV S27 and ITA1 strains in mice skeletal muscle. The values are assigned according to the number of stained cells; 0, no cells stained; 1, very few cells stained; 2, some cells stained; 3, many cells stained; 4, all cells are stained. The values obtained in the plot are the average of all the values assigned in each skeletal muscle of both strains. The muscles infected with S27 strain presented more stained tenocytes than those muscles infected with ITA1 strain, otherwise muscles infected with ITA1 strain presented more stained endothelial cells. The fibrocytes of the graph are those stained in the endo and perimysium. However, the differences between both strains were not statistically significant in tenocytes (P=0.47), fibrocytes of endo and perimysium (P=0.21), endothelial cells (P=0.72) and nerve sheath (P=0.85). Muscle fibers of the control skeletal muscle presented non-specific staining, thus, they were assigned the value 0 and the remaining cells did not show staining.

### 3.1.5. Encephalon

In mice infected by both strains, staining was observed in leptomeningeal cells and neuroglial cells (figure 14). Encephalons showed focal areas of imunolabeled glia, however, in figure 14A the Purkinje cells were not stained, as well as the mesencephalon neurons (Figure 14B). Previous studies of CHIKV models in mice (Couderc *et al.*, 2008) did not observe staining in glial cells, however in this case some stained foci were found throughout the entire brain and more foci were observed in the brain cells of mice infected with the ITA1 strain, but the differences between both strains were not statistically significant (figure 15). No staining was found in the neurons or in the endothelial cells. However, studies of CHIKV in humans have shown infection in the endothelial cells (Rougeron *et al.*, 2015) and epithelial cells in the encephalon, as well as high viremia in general.

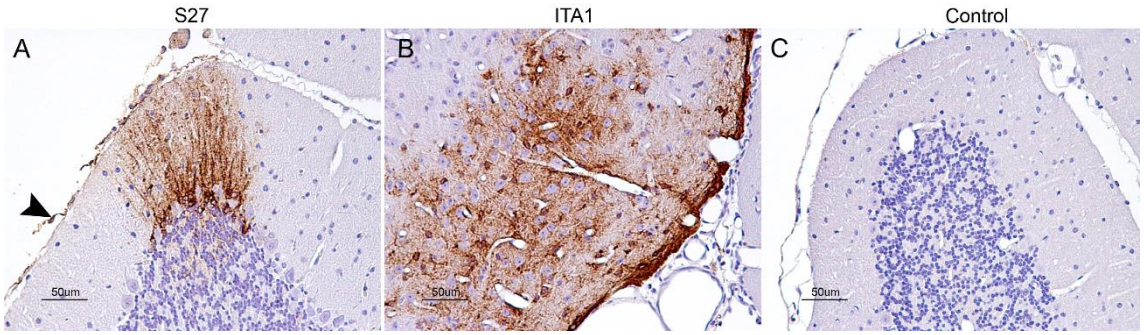


**Figure 14.** Brain tissue (cerebellum) of mice infected with $10^6$ pfu of CHIKV and control mice (50 µm). (A) Brain tissue (cerebellum) of a mouse infected with S27 strain 2DPI. It can be seen the stained leptomeninges (arrowhead) and some spots of neuroglia stained. Stained neurons were not observed. (B) Cerebellum of a mouse infected with ITA1 strain 3DPI. A big stained neuroglia spot was observed. Stained neurons were not observed. (C) Control brain tissue (cerebellum) without staining.

With the immunohistochemistry technique used in the present work, it is not possible to differentiate which specific type of neuroglia cells are those that are stained (astrocytes, oligodendrocytes or microglia cells). Some of these cells looked morphologically similar to the Bergmann's glia in the cerebellum, whereas in the focus of the mesencephalon they could be microglial cells. However, they all have been taken into account as glia in general. As for the leptomeninges a moderate and quite similar staining was observed in those brains infected with both strains (figures 14A and 14B), when compared with the control ones (figure 14C). This tropism on the meninges was described in previous studies in models with mice (Couderc *et al*., 2008), so it is confirmed again in this experiment.

Nonspecific staining of choroid plexuses cells was observed, because there were punctate intracellular immunolabeling in both infected mice and in control mice (see figures 24D, 24E, 24F in section A). Therefore, they have not been taken into account in the evaluation of results and have been considered artifacts.

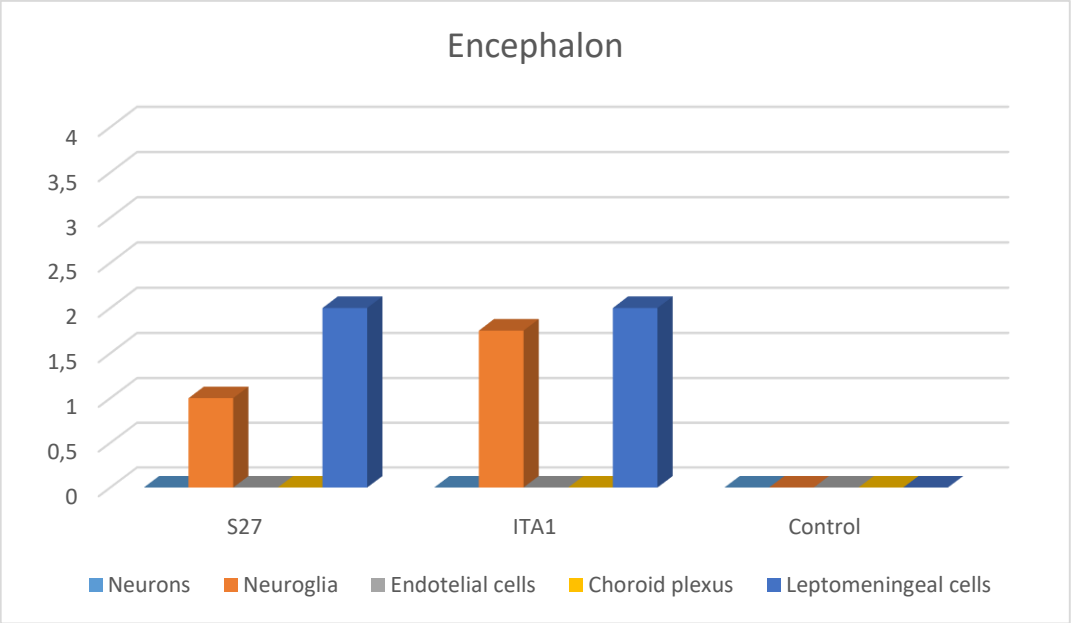


**Figure 15.** Comparative plot of CHIKV S27 and ITA1 strains in mice encephalon. The values are assigned according to the number of stained cells; 0, no cells stained; 1, very few cells stained; 2, some cells stained; 3, many cells stained; 4, all cells are stained. The values obtained in the plot are the average of all the values assigned in each encephalon of both strains. More neuroglia cells were stained in those encephalons infected with ITA1. The differences between both strains were not statistically significant in neuroglial cells (P=0.15) and leptomeningeal cells (P=1). No neurons and endothelial cells were stained. The cells of the control encephalons did not present staining, except the choroid plexuses, because they were nonspecifically stained.

### 3.1.6. Skin

Mice infected with S27 strain had some stained fibrocytes in the dermis (Figure 16A), and some cells that could be interpreted as macrophages (Langerhans cells) or fibrocytes. Mice infected with ITA1 strain also had some stained fibrocytes in the dermis, although in a smaller amount with respect to the S27 strain (figure 16B). It is known that dermis fibrocytes and fibroblasts are target cells of the virus during the acute phase of viral infection. The virus replicates in these cells and then spreads in the monocytes through the blood. Therefore, the tropism of the virus by these cells is also demonstrated in the present study. In previous studies (Couderc *et al*., 2008) immunolabeling was observed in the fibroblasts of the deep dermis, where the virus was inoculated ID. In our study, despite a different inoculation route was used (i.e. subcutaneous) a similar virus antigen distribution in the skin was observed. It should be noted that in the skins infected with S27 a few stained sebaceous glands were found (figure 17A), but not in the ITA1 strain (figure 17B), nor in control mice (figure 17C). The differences between both strains were not statistically significant (figure 18).

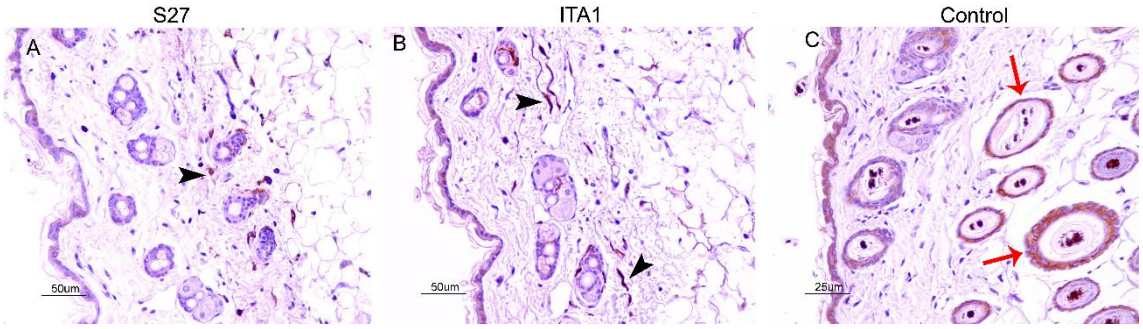


**Figure 16.** Skin tissue of mice infected with $10^6$ pfu of CHIKV and control mice (50µm). (A) Skin tissue of a mouse infected with S27 strain 2DPI. Immunostained cells (probably fibrocytes or macrophages) can be seen in the dermis (arrowhead). (B) Skin tissue of a mouse infected with ITA1 strain 3DPI. A bigger amount of stained fibrocytes can be observed than in 16A (arrowheads). (C) Control skin tissue with some non-specific staining in hair follicles (red arrows).

In infected mice skins, a lot of artefactual inmunolabeling was observed, this is because in control mice staining was observed in the epidermis hair follicles and in the keratinocytes (figures 16C and figures 24A, 24B, 24C in artifacts section). Therefore, they have not been taken into account in the evaluation of the results. On the other hand, the most remarkable staining has been observed in adipocytes, a large part of them were stained, including those that are part of the brown adipose tissue. Adipocyte inmunolabeling was also found in control mice (figures 21A, 21B and 21C in section A), so they have not been taken into account either.

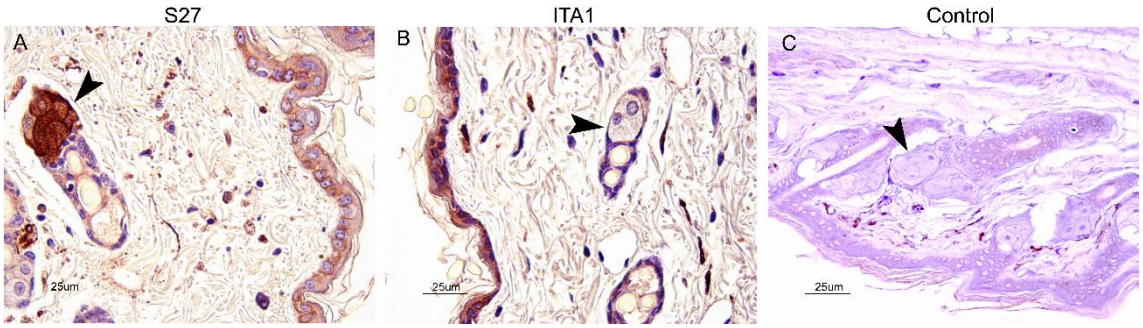


**Figure 17.** Sebaceous glands of mice infected with $10^6$ pfu of CHIKV and control mice (50µm). (A) Sebaceous gland of a mouse infected with S27 strain 2DPI. Immunolabeled glands could be clearly seen (arrowhead). (B) Unstained sebaceous gland of a mouse infected with ITA1 strain 3DPI (arrowhead). (C) Control skin tissue with unstained sebaceous glands (arrowhead).

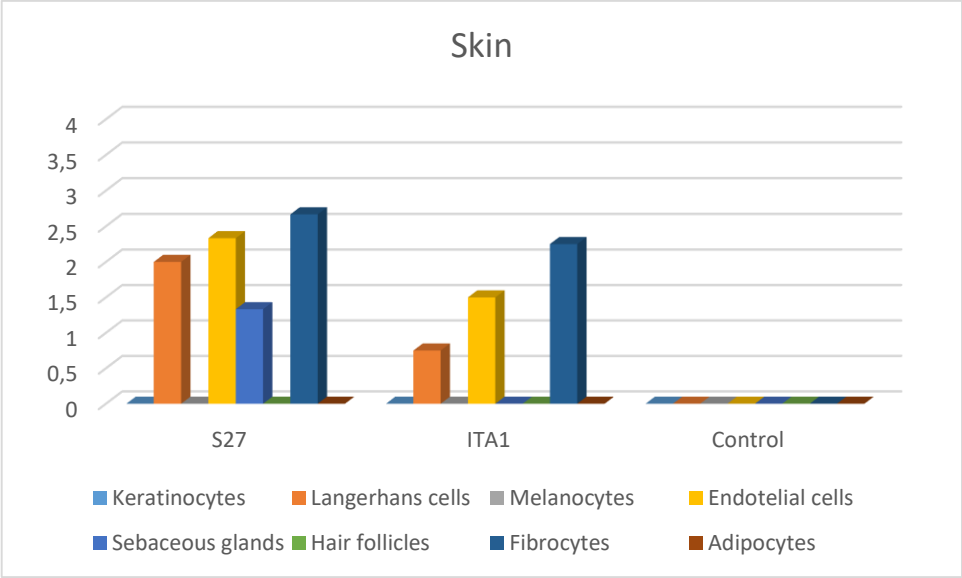


**Figure 18.** Comparative plot of CHIKV S27 and ITA1 strains in mice skin. The values are assigned according to the number of stained cells; 0, no cells stained; 1, very few cells stained; 2, some cells stained; 3, many cells stained; 4, all cells are stained. The values obtained in the plot are the average of all the values assigned in each skin of both strains. The differences between both strains were not statistically significant in macrophages (Langerhans cells) (P=0.15), endothelial cells (P=0.21), sebaceous glands (P=0.21) and fibrocytes (P=0.72). The sebaceous glands were only stained in skins infected with S27 strains. The cells of the control skins presented non-specific staining in hair follicles, keratinocytes, melanocytes and adipocytes, therefore, they were assigned the value 0 and the remaining cells did not show staining.

### 3.1.7. Joints

Joints of both knee and feet were evaluated. Even though no arthritis was observed in this model, a remarkable staining in the synoviocytes of the synovial membrane (figures 19A and 19B) was observed in both mice infected by S27 and ITA1 strains. There was no staining in control mice (figure 19C). There are two types of synoviocytes; the macrophages and the fibrocytes, according to the samples observed and the pictures it is very probable that both types of synoviocytes are immunolabeled.

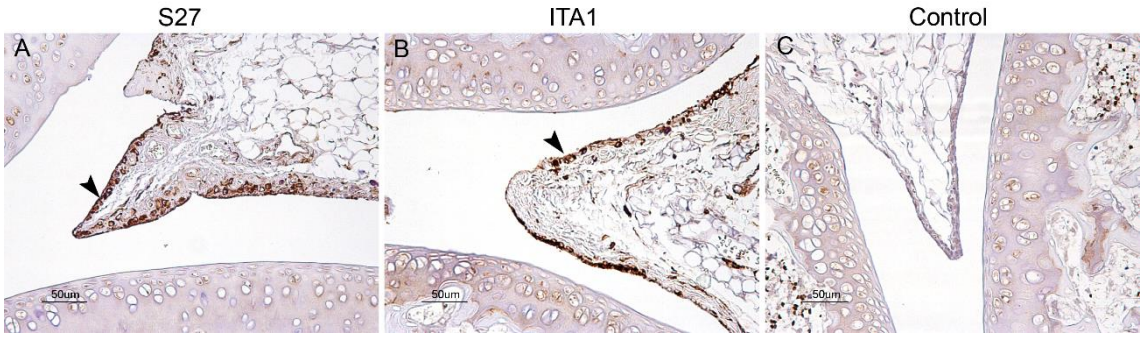


**Figure 19** Knee synovial membrane tissue of mice infected with $10^6$ pfu of CHIKV and control mice (50µm). (A)

Synovial membrane tissue of a mouse infected with S27 strain 2DPI. A large amount of fibrocytes are stained (arrowhead). (B) Synovial membrane tissue of a mouse infected with ITA1 strain 3DPI. A large amount of stained fibrocytes can be observed as well as in 16A (arrowhead). (C) Control synovial membrane tissue without staining.

CHIKV produces inflammatory arthralgia in the acute phase that can lead to severe arthritis during the chronic phase. As the virus has a marked tropism by the synovial membranes it makes sense that one of the symptoms of the disease is arthralgia/arthritis. However, more marked fibrocytes were found in those mice infected by the S27 strain than in those infected by ITA1. On the other hand, a strong tropism of the virus was also observed in the periosteum (figures 20A, 20B) that were not seen in the control mice (figure 20C), and again, more marked in mice infected by S27. Possibly it is also responsible for joint pain that occurs in this disease. As for the bones, only a few osteocytes stained in both S27 and ITA1 infected mice have been observed, however, osteoclasts and stained osteoblasts could not be clearly identified. In general, the differences between both strains were not statistically significant (figure 21).

In the bone marrow, there were found in both S27 and ITA1 infected mice some large stained hematopoietic precursor cells (Figures 20D and 20E), which were not seen in the control bone marrows (Figure 20F). However, nonspecific inmunolabeling of some bone marrow smaller cells was observed (Figure 20F), which may be due to the fact that they are hematopoietic precursors and the chromogen used may have reacted with endogenous peroxidase that has not been completely blocked.

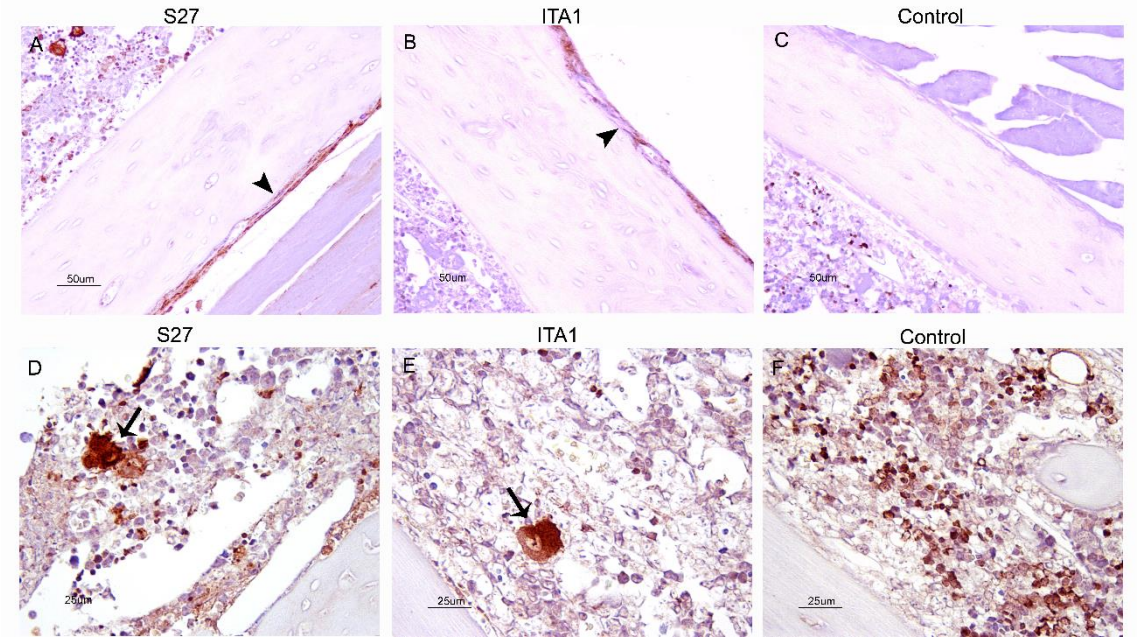


**Figure 20.** Periosteum (50 µm) and bone marrow (25 µm) of the joint of mice infected with $10^6$ pfu of CHIKV and control mice. (A) Periosteum of a mouse infected with S27 strain 2DPI. Almost all the periosteum was stained (arrowhead). (B) Periosteum of a mouse infected with ITA1 strain 3DPI, with almost all the periosteum stained

(arrowhead). (C) Control periosteum without staining. (D) Bone marrow of a mouse infected with S27 strain 2DPI. Large stained hematopoietic precursor cells could be observed (arrow). (E) Bone marrow of a mouse infected with ITA1 strain 3DPI. Large stained hematopoietic precursor cells could be observed as well (arrow). (F) Control bone marrow with some non-specific staining in hematopoietic cells.

The chondrocytes of the joints have been taken into account as an artifact in the feet of the animals, since they appeared stained both in infected animals and in control animals (figures 23D, 23E, 23F).

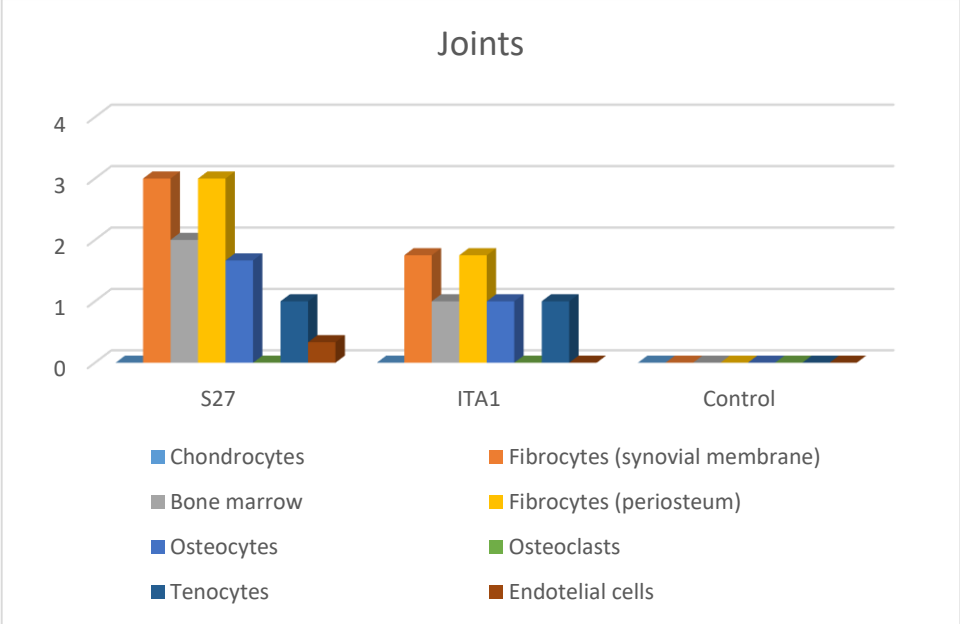


**Figure 21.** Comparative plot of CHIKV S27 and ITA1 strains in mice joint. The values are assigned according to the number of stained cells; 0, no cells stained; 1, very few cells stained; 2, some cells stained; 3, many cells stained; 4, all cells are stained. The values obtained in the plot are the average of all the values assigned in each joint of both strains. The differences between both strains were not statistically significant in fibrocytes (synovial membrane) (P=0.05), bone marrow (P=0.15), fibrocytes (periosteum) (P=0.37), osteocytes (P=0.21), tenocytes (P=0.85) and endothelial cells (P=0.59). The cells of the control joints did present nonspecific staining in chondrocytes, therefore they have not been taken into account in the evaluation of the results.

## 3.2 Comparison between two CHIKV strains

In the present work, the results obtained from each strain have been compared in Table 2, that is to say, 3 mice infected with the S27 strain 2 DPI, 1 mouse infected with the ITA1 strain 2 DPI and 3 infected mice with the ITA1 strain 3 DPI (table 2).

**Table 2**. Comparison of the results between strains S27 2DPI and ITA1 2DPI, 3DPI. The values are assigned according to the number of stained cells; (-), no cells stained; (+), very few cells stained; (++), some cells stained; (+++), many cells stained; (++++), all cells are stained. According to the results, the differences between both strains are not very remarkable. The S27 strains seems to be a bit more aggressive than ITA1.

| | | | S27 $10^6$ (2 dpi) | ITA1 $10^6$ (2 dpi) | ITA1 $10^6$ (3 dpi) |
|---|---|---|---|---|---|
| **Liver** | Kupffer cells | | ++ | ++ | ++ |
| | Endothelial cells | | ++ | + | + |
| | Fibrocytes basal lamina | | + | ++ | + |
| | Hepatocytes | | - | - | - |
| | Bile ducts | | - | - | - |
| **Spleen** | Endothelial cells | | + | + | + |
| | Fibrocytes (trabeculae) | | + | ++ | + |
| | Lymphocytes (White pulp) | | ++<br>Low lympholysis | ++<br>Severe lympholysis | +<br>Severe Lympholysis |
| | Macrophages | | +++ | ++ | ++ |
| | Lymphocytes (follicles) | | - | - | - |
| | Megakaryocytes | | + | + | + |
| **Lymph node** | Lymphocytes | | +<br>Low lympholysis | +<br>Moderate Lympholysis | +<br>Severe Lympholysis |
| | Macrophages | | ++ | ++ | + |
| | Fibrocytes | | +++ | ++ | ++ |
| | Endothelial cells | | ++ | ++ | + |
| **Skeletal muscle** | Muscle fibers | | - | - | - |
| | Tenocytes | | ++ | +++ | + |
| | Endothelial cells | | ++ | +++ | ++ |
| | **Nerve sheath** | Nerve fibers | - | - | - |
| | | Schwann cells | + | - | - |
| | | Fibrocytes | +++ | +++ | ++ |
| **Encephalon** | Neurons | | - | - | - |
| | Neuroglia (oligodendrocytes, astrocytes, microglia) | | + | ++ | ++ |
| | Ependymal cells | | - | - | - |
| | Endothelial cells | | - | - | - |
| | Choroid plexuses | | - | - | - |
| | Leptomeningeal cells | | ++ | ++ | ++ |
| **Skin** | Keratinocytes | | - | - | - |
| | Langerhans cells | | ++ | ++ | ++ |
| | Melanocytes | | - | - | - |
| | Endothelial cells | | ++ | ++ | + |
| | Sebaceous glands | | + | - | - |
| | Hair follicles | | - | - | - |
| | Fibrocytes | | +++ | +++ | ++ |
| | Adipocytes | | - | - | - |
| **Joint** | Chondrocytes | | - | - | - |
| | Fibrocytes (sinovial membrane) | | +++ | ++ | ++ |
| | Bone marrow | | ++ | + | + |
| | Fibrocytes (periosteum) | | +++ | +++ | +++ |
| | Osteocytes | | + | + | + |
| | Osteoclasts | | - | - | - |
| | Tenocytes | | + | - | + |
| | Endothelial cells | | + | - | - |

.

According to the results observed, both strains do not show very clear differences in terms of cellular and tissue tropism of the CHIKV. However, it appears that the S27 strain is capable of infecting more cells in general, for example, the macrophages of the spleen or lymph node and the fibrocytes of the basal lamina and synovial membrane, even though the results were not statistically significant. The S27 strain was more virulent than ITA1 because at the same dose of the virus mice died earlier. On the other hand, the ITA1 strain causes more lympholysis than the S27 strain, this could be clearly seen in the spleen of the mice and in the lymph node. In the spleen, the lymphoid depletion by ITA1 strain was quite similar to both 2 DPI and 3 DPI, however, there was more difference between 2 DPI and 3 DPI in the lymph node. In ITA1 (3 DPI), lympholysis was greater.

This is a good model to study the acute phase of the disease, but not chronic phases. Mice have died during the acute phase and in the original model no lesions were observed such as encephalitis, arthritis and myositis. Therefore, it do not reproduce the viral infection in humans.

## 4. Conclusions

1. The characterization of cellular tropism of two strains of CHIKV has been established in a mouse IFN-α/β $^{(-/-)}$ receptor knock out model showing presence of viral antigen in macrophages, endothelial cells, fibrocytes, lymphocytes, megakaryocytes, tenocytes, neuroglial cells, leptomeningeal cells, osteocytes and some cells of the bone marrow.

2. When comparing the S27 and ITA1 strains in the infected mice, no significant differences were observed between them.

3. Most of the cells identified with the virus had already been described in previous studies, although in this case some differences have been observed.

3.1. Immunolabeling has been found in the periosteum of the bones, sebaceous glands of skins infected by S27 strain, some cells of the bone marrow and foci of glia cells in the encephalon.

3.2. No immunolabeling was found in endothelial cells or choroid plexus of the encephalon as in previous studies.

4. Even though different CHIKV strains and, specially, a different inoculation route (subcutaneous instead of intradermal) was used here in comparison to other studies our models displays a very similar virus tropism.

5. Despite the absence of typical CHIKV lesions such as arthritis or encephalitis, the virus tropism for this tissues is confirmed in this model. Thus, it makes it suitable for further pathogenesis studies.

## Annex: Artifacts

In the performance of this experiment, non-specific staining was observed in some tissues, since that staining was observed in both infected mice and control mice. This is one of the most common problems in immunohistochemistry and it could be due to several causes. Unwanted background staining may occur when the tissue epitope has moved away from its sites of synthesis into the surrounding tissue. Because many fixatives penetrate tissues slowly, it is important to keep tissue specimens as small as possible and to fix immediately. Otherwise the antigens may not be adequately fixed and may be extracted or displaced by the subsequent tissue processing steps (Taylor *et al*., 2013).

Polymer-based detection systems may induce general non-specific staining if insufficient washing is performed after polymer application. Due to the large size of some polymer conjugates, the diffusion rate of these molecules is lower than for low-molecular weight conjugates. However, this can be resolved by applying multiple wash steps, adding detergent to the wash buffer, and by prolonging washing time.

Another reason why non-specific staining occurs is cross-reactivity. It may result when target tissue antigen epitopes are shared with other proteins. It may also be the cause of confusing background staining.

Finally, other situations that may occur is that in the tissues were some endogenous peroxidases that were not eliminated in the blocking step. The DAB reacts with these peroxidases resulting in tissue staining in unexpected places. The solution to this problem could be to use a different visualization system.

Some examples of these nonspecific stains are shown below in the figures 22, 23, 24 and 25. Immunohistochemistry techniques may have problems regarding the interpretation of the results. The use of control animals in this sort of experiments is important because it allows to distinguish which staining is artifactual and which is specific staining. Thus, in the final interpretations controls must be taken into account to get reliable results.

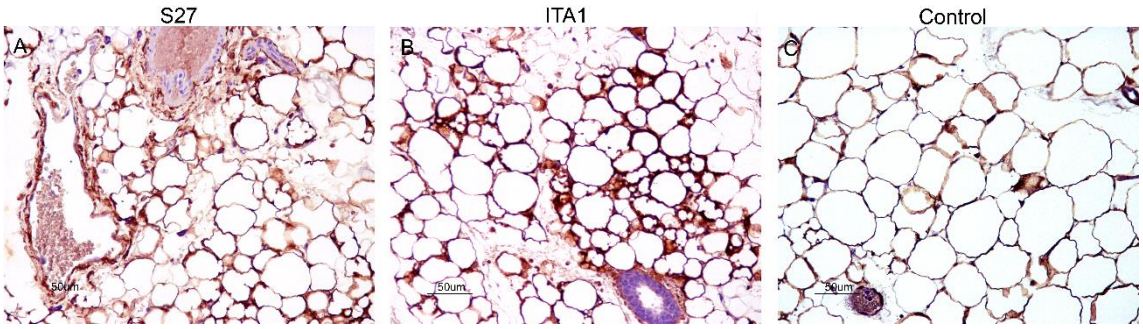


**Figure 22.** Adipocytes unspecifically stained of mice infected with $10^6$ pfu of CHIKV (50 µm). (A, B, C) Non-specific stained adypocites, they are stained in both infected mice and in control mice.

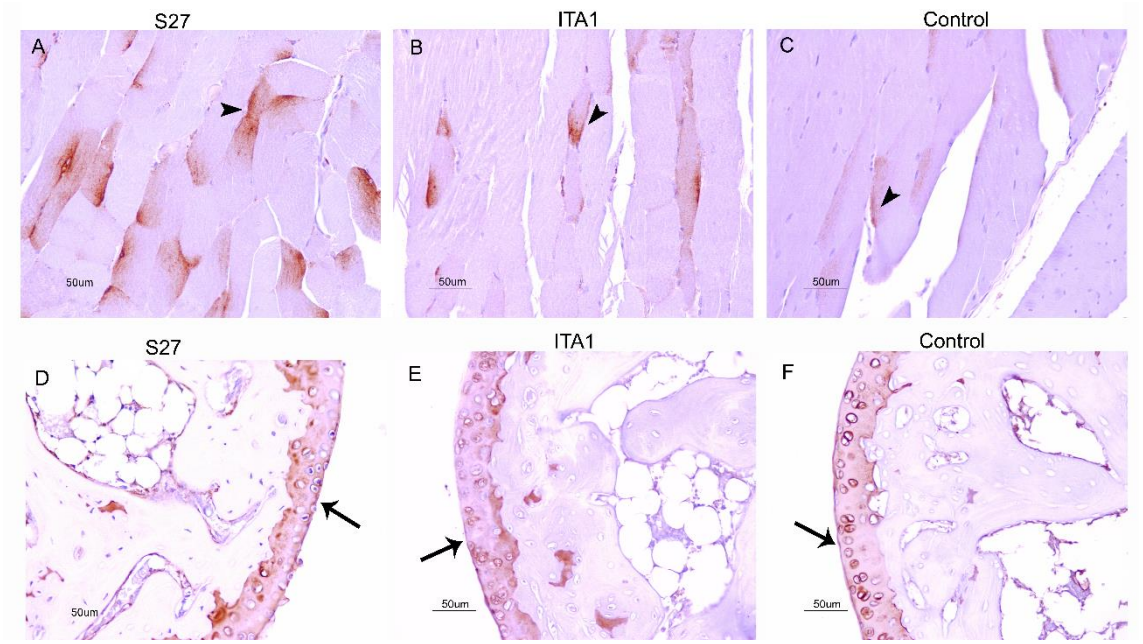


**Figure 23.** Skeletal muscle and cartilage nonspecifically stained of mice infected with $10^6$ pfu of CHIKV (50 µm). (A, B, C) Nonespecifically stained muscle fibers because they are stained in both infected mice and in control mice (arrowheads). (D, E, F) Nonespecifically stained cartilage because they are stained in both infected mice and in control mice (arrows).

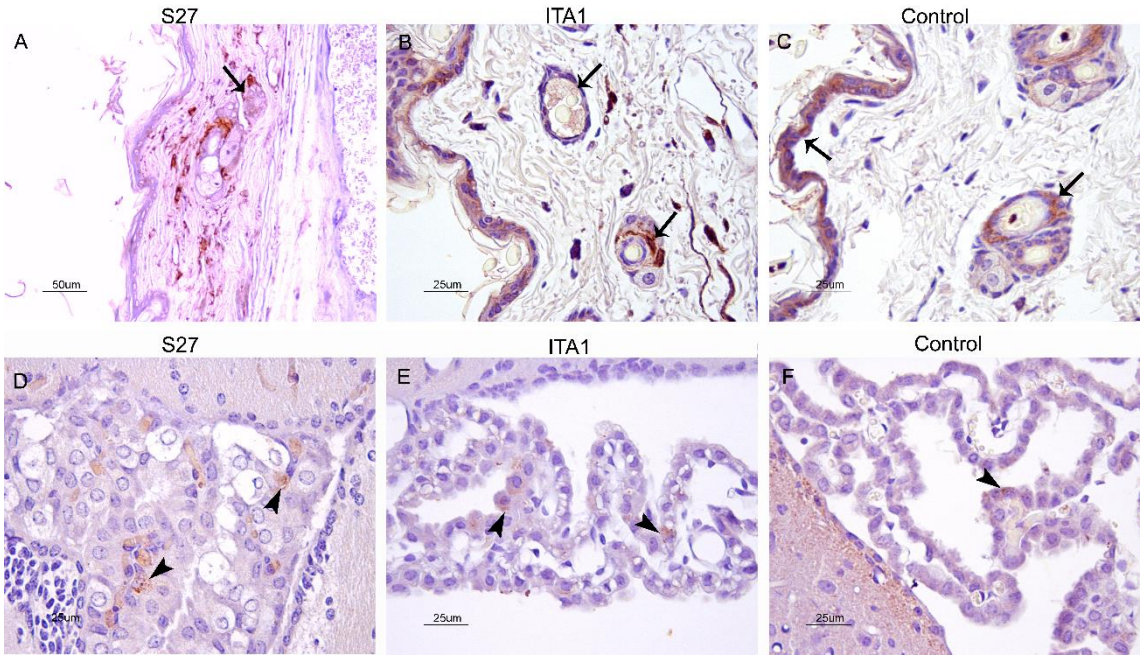


**Figure 24.** Skin and choroid plexuses unspecifically stained of mice infected with $10^6$ pfu of CHIKV (25µm). (A, B, C) Non-specific stained keratinocytes and hair follicles, they are stained in both infected mice and in control mice (arrows). (D, E, F) Non-specific stained choroid plexuses, they are stained in both infected mice and in control mice (arrowheads).

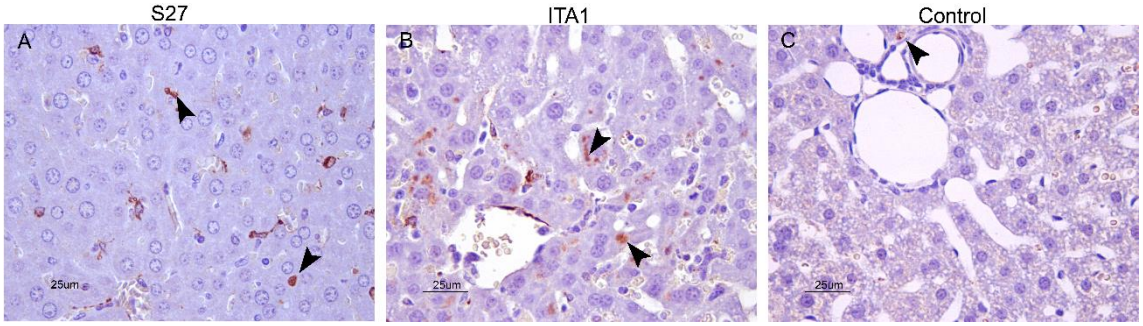


**Figure 25.** Non-specific intracytoplasmatic staining in the hepatocytes of mice infected with $10^6$ pfu of CHIKV (25 µm). (A, B, C) Non-specific stained hepatocytes, they are stained in both infected mice and in control mice.

## References

[1] An W., Ge N., Cao Y., Sun J., Jin X. (2017). *Recent progress on chikungunya virus research*. *Virologica Sinica*. Vol. **32** (6), 441-453.

[2] Burt F.J., Chen W., Miner J.M., Lenschow D.J., Merits A., Schnettler E, Kohl A., Rudd P.A., Taylor A., Herrero L.J., Zaid A., F PNg L., Mahalingam S. *Chikungunya virus: an update on the biology and pathogenesis of this emerging pathogen*. *The Lancet Infectious Disease*. Vol **17**, 107-117.

[3] Cirimotich, C.M., Vela, E.M., Garver, J., Barnewall, R.E., Miller, B.D., Meister, G.T., Rogers, J.V., (2017). *Chikungunya virus infection in Cynomolgus macaques following Intradermal and aerosol exposure*. Virology Journal. Available online on: https://virologyj.biomedcentral.com/articles/10.1186/s12985-017-0804-7 (published on July 20, 2017, consulted on May 11, 2018).

[4] Couderc, T., Chrétien F., Schilte C., Disson, O., Brigitte, M., Guivel-Benhassine, F., Touret, Y., Barau, G., Cayet, N., Schuffenecker, I., Desprè, P., Arenzana-Seisdedos, F., Michault, A., Albert, M.L., Lecuit, M., (2008). *Mouse Model for Chikungunya: Young Age and Inefficient Type-I Interferon Signaling Are Risk Factors for Severe Disease.* PloS Pathogens. Vol. **4**, Issue 2, 1-12.

[5] Fernandez-Garcia M.D., Bangert M., de Ory F., Potente A., Hernandez L., Lasala F., Herrero L., Molero F., Negredo A., Vázquez A., Minguito T., Balfagón P., de la Fuente J., Puente S., Ramírez de Arellano E., Lago M., Martinez M., Gascón J., Norman F., Lopez-Velez R., Sulleiro E., Pou D., Serre N., Roblas R.F., Tenorio A., Franco L., Sanchez-Seco M.P., (2016). *Chikungunya virus infections among travellers returning to Spain, 2008 to 2014*. Euro Surveill. 2016; 21(36):pii=30336. DOI: http://dx.doi.org/10.2807/1560-7917.ES.2016.21.36.30336

[6] Ganesan, V.K., Duan, B. and Reid, St P. *Chikungunya Virus: Pathophysiology, Mechanism, and Modeling* (2017). *Viruses*. Vol **9**, 1-14.

[7] Labadie, K., Larcher, T., Joubert, C., Mannioui, A., Delache, B., Brochard, P., Guigand, L., Dubreil, L., Lebon, P., Verrier, B., Lamballerie, X., Suhrbier, A., Cherel, Y., Le Grand,

R., and Roques, P., (2010). *Chikungunya disease in nonhuman primates involves long-term viral persistence in macrophages*. The Journal of Clinical Investigation. Vol. **120**, 894-906.

[8] Lisa F.P.Ng (2017). *Immunopathology of Chikungunya Virus Infection: Lessons Learned from Patients and Animal Models.* Annual Review Virology. Vol. **4**, 413–27.

[9] Rougeron, V., Sam, I.C., Caron, M., Nkoghe, D., Leroy, E., Roques P., (2015). *Chikungunya, a paradigm of neglected tropical disease that emerged to be a new health global risk*. Journal of Clinical Virology. Vol. **64**, 144-152.

[10] Schwartz, O. and Albert, M.L. *Biology and pathogenesis of chikungunya virus* (2010).*Nature Reviews*. Vol **8**, 491-500.

[11] Staples, J.E., Breiman, R.F., and Powers, A.M. (2009). *Chikungunya Fever: An Epidemiological Review of a Re-Emerging Infectious Disease*. *Emerging Infectious Diseases*. Vol. **49**, 942-948.

[12] Taylor, C.R., Rudbeck, L., Sjørup, A. H. (2013). Inmunohistochemical Staining Methods. Dako Denmark A/S, an Agilent Technologies Company. 170-179.

[13] Wahida, B., Alia, A., Rafiquea, S., Idrees, M., (2017). *Global expansion of chikungunya virus: mapping the 64-year history*. International Journal of Infectious Diseases. Vol. **58**, 69-76.

[14] Weetman, D., Kamgang, B., Badolo, A., Moyes, C.L., Shearer, F.M., Coulibaly, M., Pinto, J., Lambrechts, L., McCall, P.J., (2018). *Aedes Mosquitoes and Aedes-Borne Arboviruses in Africa: Current and Future Threats*. International Journal of Environmental Research and Public Health. Vol. **15**(2), 220.

[15] Whitehead, S.S., Blaney J.E., Durbin A.P., Murphy, B.R., (2007). *Prospects for a dengue virus vaccine*. Nature reviews. Vol.**5**, 518-528.

[16] Ziegler, S.A., Lu, L., Tavassos da Rosa, A.P.A, Xiao, S.Y., Tesh, R.B (2008). *An Animal Model for Studying the Pathogenesis of Chikungunya Virus Infection.* The American Journal of Tropical Medicine and Hygene. Vol. **79**, 133-129.